



Original Contribution

Oxidative damage in human gingival fibroblasts exposed to cigarette smoke

Graziano Colombo ^{a,1}, Isabella Dalle-Donne ^{a,*,1}, Marica Orioli ^b, Daniela Giustarini ^c, Ranieri Rossi ^c, Marco Clerici ^{a,d}, Luca Regazzoni ^b, Giancarlo Aldini ^b, Aldo Milzani ^a, D. Allan Butterfield ^{e,f,g}, Nicoletta Gagliano ^d

^a Department of Biology, Università degli Studi di Milano, I-20133 Milan, Italy

^b Dipartimento di Scienze Farmaceutiche "Pietro Pratesi," Università degli Studi di Milano, I-20133 Milan, Italy

^c Department of Evolutionary Biology, University of Siena, I-53100 Siena, Italy

^d Department of Human Morphology and Biomedical Sciences "Città Studi," Università degli Studi di Milano, I-20090 Segrate, Milan, Italy

^e Department of Chemistry, University of Kentucky, Lexington, KY 40506, USA

^f Center of Membrane Sciences, University of Kentucky, Lexington, KY 40506, USA

^g Sanders-Brown Center on Aging, University of Kentucky, Lexington, KY 40506, USA

ARTICLE INFO

Article history:

Received 4 November 2011

Revised 14 February 2012

Accepted 16 February 2012

Available online 1 March 2012

Keywords:

Cigarette smoke

Redox proteomics

Human gingival fibroblasts

Protein carbonylation

Protein thiols

GSH- α,β -unsaturated aldehyde adducts

Free radicals

ABSTRACT

Cigarette smoke, a complex mixture of over 7000 chemicals, contains many components capable of eliciting oxidative stress, which may induce smoking-related disorders, including oral cavity diseases. In this study, we investigated the effects of whole (mainstream) cigarette smoke on human gingival fibroblasts (HGFs). Cells were exposed to various puffs (0.5–12) of whole cigarette smoke and oxidative stress was assessed by 2',7'-dichlorofluorescein fluorescence. The extent of protein carbonylation was determined by use of 2,4-dinitrophenylhydrazine with both immunocytochemical and Western immunoblotting assays. Cigarette smoke-induced protein carbonylation exhibited a puff-dependent increase. The main carbonylated proteins were identified by means of two-dimensional electrophoresis and MALDI-TOF mass spectrometry (redox proteomics). We demonstrated that exposure of HGFs to cigarette smoke decreased cellular protein thiols and rapidly depleted intracellular glutathione (GSH), with a minimal increase in the intracellular levels of glutathione disulfide and S-glutathionylated proteins, as well as total glutathione levels. Mass spectrometric analyses showed that total GSH consumption is due to the export by the cells of GSH-acrolein and GSH-crotonaldehyde adducts. GSH depletion could be a mechanism for cigarette smoke-induced cytotoxicity and could be correlated with the reduced reparative and regenerative activity of gingival and periodontal tissues previously reported in smokers.

© 2012 Elsevier Inc. All rights reserved.

Despite the large body of epidemiological evidence that exists today establishing a strong correlation between smoking and disease, such as lung respiratory [1] and cardiovascular disorders [2], various types of cancer [3], and oral cavity disorders [4,5], the molecular

mechanisms of smoke-related disorders and how smoking initiates and/or enhances diseases often remain unclear.

There are many harmful components in both mainstream (i.e., the smoke inhaled by active smokers, emitted at the mouthpiece of a cigarette) and sidestream (i.e., the smoke emanating from the cigarette between puffs; it is the main component (85%) of second-hand, or environmental, tobacco smoke, also known as passive, or involuntary, smoking) cigarette smoke that can damage cellular molecules, eventually leading to cell death. Two major phases were identified in whole cigarette smoke, a complex mixture of over 7000 chemical compounds [6]: a tar phase and a gas phase. Both phases are rich in reactive oxygen species (ROS) and reactive nitrogen species [7,8]. It was estimated that a single cigarette puff contains approximately 10^{14} free radicals in the tar phase and 10^{15} radicals in the gas phase [9]. In agreement with the concept that oxidative stress, an imbalance between oxidants and antioxidants in favor of the oxidants, leading to a disruption of redox signaling and control and/or molecular damage [10], is capable of causing tissue damage and disease states [10],

Abbreviations: biotin-HPDP, N-(6-(biotinamido)hexyl)-3'-(2'-pyridylidithio)propionamide; DAPI, 4',6-diamidino-2-phenylindole; DCF, 2',7'-dichlorofluorescein; DCFH-DA, 2',7'-dichlorodihydrofluorescein diacetate; DMEM, Dulbecco's modified Eagle's medium; DNPH, 2,4-dinitrophenylhydrazine; ECL, enhanced chemiluminescence; FITC, fluorescein isothiocyanate; GAPDH, glyceraldehyde-3-phosphate dehydrogenase; GSH-ACR, GSH adduct with acrolein; GSH-CRO, GSH adduct with crotonaldehyde; HGF, human gingival fibroblasts; HSA, human serum albumin; mBrB, monobromobimane; NEM, N-ethylmaleimide; PVDF, polyvinylidene difluoride; ROS, reactive oxygen species; streptavidin-HRP, streptavidin-horseradish peroxidase conjugate; TCA, trichloroacetic acid; TPM, total particulate matter.

* Corresponding author. Fax: +39 02 50314781.

E-mail address: quack@unimi.it (I. Dalle-Donne).

¹ These authors contributed equally to this work.

oxidative stress seems to play a central role in cigarette smoke-mediated diseases [e.g., 11,12]. Cigarette smoke can also induce the production of endogenous oxidants and reactive species in an inflammatory response to smoke-induced irritation [13].

Additional harmful constituents of tobacco smoke are highly reactive, volatile aldehydes, including α,β -unsaturated chemicals such as acrolein (2,3-propenal) and crotonaldehyde (2-butenal) [7]. Acrolein is present in very high concentrations in the vapor phase of all cigarettes, its levels varying up to 10-fold between high-tar and ultra-low-tar cigarette smoke extracts. Several reports have estimated that between 100 and 600 μg of acrolein is generated per cigarette (50–70 ppm) and that acrolein constitutes 50–60% of total vapor-phase electrophiles [14]. Cigarette smoke extracts from commercial cigarettes containing the average tar content of 15 mg yielded $394 \pm 29 \mu\text{mol/L}$ acrolein [15]. Extracts of different ultralights and light commercial cigarettes all yielded between 311 and 370 $\mu\text{mol/L}$ acrolein and corresponding levels of other aldehydes, indicating a lack of correlation between the purported lightness of the tobacco and the level of acrolein [15]. Smoking one cigarette per cubic meter of air of room space in 10–13 min (10 puffs) generates acrolein levels up to 0.84 mg/m^3 [16]. The respiratory tract is commonly exposed to a range of α,β -unsaturated aldehydes from cigarette smoke exposure. It was estimated that, during cigarette smoking, acrolein concentrations at the airway surface may be as high as 80 μM [17]. α,β -Unsaturated aldehydes are present in saliva and airway secretions in low-micromolar concentrations in healthy subjects and are elevated up to 10-fold in heavy smokers [18,19]. The common feature of these α,β -unsaturated aldehydes is the presence of an unsaturated carbonyl group that confers them the capacity to form stable covalent adducts with nucleophilic amino acids (i.e., Cys, His, and Lys), often resulting in protein carbonylation, as well as with the thiol group in glutathione (GSH) [20–23].

Oral cavity tissues are the first exposed to mainstream cigarette smoke and their responses to harmful stimuli are critical in maintaining periodontal homeostasis. Cigarette smoke is a known modulator of various oral cavity pathologies, but the mechanism(s) by which cigarette smoke constituents affect gingival fibroblast integrity needs to be elucidated. In this study, we exposed cultured human gingival fibroblasts (HGFs) to increasing puffs of whole (mainstream) cigarette smoke and assessed changes in protein carbonylation and intracellular total glutathione as well as formation of both intracellular and extracellular GSH- α,β -unsaturated aldehyde adducts.

Materials and methods

Materials

An HPLC Zorbax Eclipse XDB-C18 column (4.6 \times 150 mm, 5 μm) was purchased from Agilent Technologies Italia S.p.A. (Cernusco sul Naviglio, Milan, Italy). HPLC-grade and analytical-grade organic solvents were purchased from Sigma-Aldrich (Milan, Italy) or from BDH (Poole, England). HPLC-grade water was prepared with a Milli-Q water purification system. EFBA (eptafluorobutyric acid), L-glutathione, and protease inhibitor cocktail (leupeptin, aprotinin, pepstatin, and phenylmethylsulfonyl fluoride) were purchased from Sigma-Aldrich. Acrolein and crotonaldehyde were purchased from Fluka (Buchs, Switzerland). H-Tyr-His-OH (TH) was a generous gift from Flamma S.p.A. (Chignolo d'Isola, Bergamo, Italy). Monobromobimane (mBrB) was obtained from Calbiochem (La Jolla, CA, USA). EZ-Link biotin-HPDP (*N*-(6-(biotinamido)hexyl)-3'-(2'-pyridyl)dithio)propionamide) was obtained from Thermo Scientific (Rockford, IL, USA). Anti-dinitrophenyl-KLH (anti-DNP) antibodies, rabbit IgG fraction, goat anti-rabbit IgG, horseradish peroxidase conjugate, and 2',7'-dichlorodihydrofluorescein diacetate (DCFH-DA) were purchased from Molecular Probes (Eugene, OR, USA). Monoclonal anti-GSH antibody was obtained from Virogen (Watertown, MA, USA). Goat anti-rabbit fluorescein isothiocyanate (FITC) conjugate

was purchased from Santa Cruz Biotechnology (Santa Cruz, CA, USA). Precision Plus Protein All Blue standards, ranging from 10 to 250 kDa, were obtained from Bio-Rad Laboratories s.r.l. (Segrate, Italy). Sheep anti-mouse IgG, horseradish peroxidase conjugate, Amersham ECL Plus Western blotting detection reagents, and streptavidin-horseradish peroxidase conjugate (streptavidin-HRP) were purchased from GE Healthcare Europe GmbH (Milan, Italy). Research-grade cigarettes (3R4F) were purchased from the College of Agriculture, Kentucky Tobacco Research and Development Center, University of Kentucky (Lexington, KY, USA). According to the analysis of 3R4F reference cigarettes preliminarily performed by the College of Agriculture Reference Cigarette Program, University of Kentucky, and further confirmed in a recent study [24], the average values (mean \pm SD) for standard parameters for the smoke of 3R4F reference cigarettes are total particulate matter $11.0 \pm 0.33 \text{ mg/cigarette}$, tar (nicotine-free dry particulate matter) $9.4 \pm 0.56 \text{ mg/cigarette}$, nicotine $0.73 \pm 0.04 \text{ mg/cigarette}$, and carbon monoxide $12.0 \pm 0.6 \text{ mg/cigarette}$.

Cell culture and cell viability assay

HGFs were obtained by a gingival biopsy from a young healthy subject, who had clinically normal gums, with no signs of inflammation or hyperplasia. Health, drugs, alcohol abuse, and smoking histories were considered as exclusion criteria. The donor gave his informed consent to the biopsy, which was obtained from adherent gums under local anesthesia during minor oral surgical procedures. The gingival tissue fragment was extensively washed with sterile phosphate-buffered saline (PBS), plated in T-25 flasks, and incubated in Dulbecco's modified Eagle's medium (DMEM) supplemented with 10% heat-inactivated fetal bovine serum and antibiotics (100 U/ml penicillin, 0.1 mg/ml streptomycin) at 37 °C in a humidified atmosphere containing 5% CO₂. When fibroblasts grew out from the explant, they were trypsinized (0.25% trypsin–0.2% EDTA) for secondary cultures. Viability was assessed by the trypan blue exclusion method. Confluent HGFs were used at the fifth passage.

Exposure of human gingival fibroblasts to cigarette smoke

HGFs were exposed to mainstream cigarette smoke using a homemade smoking device, consisting in a system connected to the tissue culture flask, to the cigarette, and to a 60-ml syringe. By regulating the system with a valve, it is possible to aspirate the cigarette smoke using the syringe and then to deliver the smoke into the flask. The use of the syringe allows one to aspirate and to deliver a precise and fixed quantity of smoke into the flask, quantified as number of "puffs." One single puff corresponds to a 60-ml volume of cigarette smoke aspirated into the syringe; 12 puffs correspond to one cigarette. Before the connection to the smoking device, the HGFs were washed with sterile PBS. The washing PBS was replaced with 1 ml of sterile PBS and each flask was exposed to 0.5, 2, 5, or 12 puffs for 1 min or left untreated (control). Each treatment was performed in triplicate. In preliminary experiments, cell-free T-25 flasks containing 1 ml of sterile PBS were exposed to 0.5, 2, 5, or 12 puffs for 1 min; the smoke-exposed buffer was then recovered from each flask and the smoke delivery system was validated by measuring the absorbance at a wavelength of 340 nm. The absorbance measured at A₃₄₀ showed insignificant variation between flasks exposed to the same number of cigarette puffs.

Total particulate matter mass in mainstream smoke

Total particulate matter (TPM) was collected by passing the mainstream smoke of two cigarettes through a 19-mm glass fiber filter pad and that of four cigarettes through cellulose/acetate filter pads (one cigarette per filter pad). The smoking protocol was the same as that used to expose HGFs to cigarette smoke. To estimate TPM mass,

each filter was weighed in triplicate both before and after sampling and desiccation using a microbalance. The difference between the final average mass of the sample filter and the initial average mass of the blank filter was used as the TPM mass. We measured a TPM mass of 11.6 mg/cigarette using the glass fiber filter pad and 11.33 ± 0.78 mg/cigarette using cellulose/acetate filter pads.

Detection of intracellular ROS formation with DCFH-DA dye assay

DCFH-DA was prepared as a 3.33 mM stock solution in absolute ethanol. Control and smoke-treated HGFs were washed in PBS and incubated in the dark for 45 min, at 37 °C, in complete DMEM containing DCFH-DA at the final concentration of 10 μ M. The cells were then washed with serum-free medium and maintained in 1 ml of serum-free culture medium. Cellular fluorescence was monitored by an inverted microscope (Leica DMIL) at wavelengths of 480 (excitation) and 527 (emission); images were captured by a Leica DFC420 digital camera.

Immunocytochemical detection of protein carbonyls

Control and smoke-treated HGFs were cultured on 12-mm-diameter round coverslips put into 24-well culture plates. When the cells were attached, they were washed in PBS, fixed in 4% paraformaldehyde in PBS, containing 2% sucrose, for 5 min at room temperature and postfixed in 70% ethanol. The cells were then washed three times in PBS and incubated with 2,4-dinitrophenylhydrazine (DNPH; 0.1% v/v in 2 M HCl) for 1 h. After DNPH derivatization, the cells were washed four times with PBS and incubated with anti-DNP antibodies (1:500 in PBS) for 1 h at room temperature. The secondary antibody was a goat anti-rabbit FITC conjugate, diluted 1:200 in PBS and incubated for 1 h at room temperature. Negative control cells were incubated omitting the primary antibody. After the labeling procedure was completed, the coverslips were mounted onto glass slides using a mounting medium containing 4',6-diamidino-2-phenylindole (DAPI). The cells were photographed by a digital camera connected to a microscope (Nikon Eclipse E600).

Detection of protein carbonylation and protein S-glutathionylation by SDS-PAGE and Western blotting

Control and smoke-treated HGF were washed twice with PBS and harvested by trypsinization. Total cellular proteins were obtained from each flask by addition of ice-cold lysis buffer (50 mM Tris-HCl, pH 7.4, 150 mM NaCl, 5 mM EDTA, 1% Triton X-100; 1×10^6 cells/100 μ l) supplemented with protease inhibitors and 5 mM N-ethylmaleimide (NEM). The lysates were incubated on ice for 30 min and centrifuged at 14,000g, for 10 min, at 4 °C, to remove cell debris. Total cellular proteins were fractionated on 12.5% (w/v) reducing (carbonylated proteins) or nonreducing (S-glutathionylated proteins) SDS-PAGE gels and electroblotted onto a polyvinylidene difluoride (PVDF) membrane. Protein carbonylation was detected, after derivatization with DNPH, with anti-DNP antibodies specific for the 2,4-dinitrophenyl hydrazone-protein adduct by Western blot immunoassay as previously reported [25]. Protein S-glutathionylation was detected with monoclonal anti-GSH antibody by Western blot immunoassay as previously reported [26,27]. Immunostained protein bands were visualized by enhanced chemiluminescence (ECL) detection. Protein bands on PVDF membranes were then visualized by washing the blots extensively in PBS and then staining with amido black.

Two-dimensional gel electrophoresis

Each sample containing 200 μ g proteins was precipitated using a chloroform/methanol protocol and resuspended in a solution containing 7 M urea, 2 M thiourea, and 4% 3-((3-cholamidopropyl)-

dimethylammonio)-1-propanesulfonate (Chaps). Solubilized samples were used to rehydrate immobilized pH gradient (IPG) strips just before isoelectrofocusing.

For the first-dimension electrophoresis, samples were applied to IPG strips (11 cm, pH 3–10 linear gradient; GE Healthcare). Strips were rehydrated at 20 °C for 1 h without current and for 12 h at 30 V in a buffer containing 7 M urea, 2 M thiourea, 4% Chaps, 1 mM dithiothreitol (DTT), and 1% IPG buffer 3–10 (GE Healthcare). Strips were focused at 20 °C for a total of 70,000 V/h at a maximum of 8000 V using the Ettan IPGphor II system (GE Healthcare). The focused IPG strips were stored at -80 °C until second-dimension electrophoresis was performed.

For the second dimension, IPG strips were equilibrated at room temperature for 15 min in a solution containing 6 M urea, 2% SDS, 30% glycerol, 50 mM Tris-HCl (pH 8.8), and 10 mg/ml DTT and then reequilibrated for 15 min in the same buffer containing 25 mg/ml iodoacetamide in place of DTT. The IPG strips were placed on top of a 12.5% polyacrylamide gel and proteins were separated at 25 °C with a prerun step at 20 mA/gel for 1 h and a run step at 30 W/gel for 3.5 h. After run, gels were fixed and stained with Sigma ProteoSilver Plus silver stain according to the manufacturer's specifications (Sigma-Aldrich).

Western blot analysis with anti-DNP antibody

Carbonylated proteins were detected by Western immunoblotting using anti-DNP antibodies as previously reported [25] and visualized with ECL detection.

In-gel trypsin digestion

Protein spots were manually excised from silver-stained gels with a razor blade, chopped into 1-mm³ pieces, and collected into a LoBind tube (Eppendorf). Gel pieces were destained with silver destaining solutions (ProteoSilver Plus Kit; Sigma-Aldrich), washed with 100 μ l of 50% (v/v) acetonitrile in 50 mM ammonium bicarbonate (pH 7.4), dehydrated in 100 μ l of acetonitrile for 5 min, and completely dried in a Speed-Vac (ThermoSavant) after solvent removal. Digestion was performed for 2 h at 37 °C with sequencing-grade modified trypsin diluted in ProteaseMAX surfactant (Promega, Madison, WI, USA), which improves recovery of longer peptides providing an increased sequence coverage. Digested samples were centrifuged at 16,000g for 10 s and the digestion reaction with extracted peptides was transferred into a new tube. Trifluoroacetic acid was added to a final concentration of 0.5% to inactivate trypsin. Finally, samples were reduced (to ≈ 5 μ l) in a Speed-Vac and immediately analyzed.

Protein identification by matrix-assisted laser desorption/ionization-time of flight (MALDI-TOF) MS analysis

One-microliter aliquots of the trypsin-digested protein supernatant were used for MS analysis on an Autoflex MALDI-TOF (Bruker) mass spectrometer. Peak list was obtained by peak deisotoping. Spectra were accumulated over a mass range of 750–4000 Da. Alkylation of cysteine by carbamidomethylation and oxidation of methionine were considered fixed and variable modifications, respectively. Two missed cleavages per peptide were allowed, and an initial mass tolerance of 50 ppm was used in all searches. Peptides with masses corresponding to those of trypsin and matrix were excluded from the peak list. Proteins were identified by searching against a comprehensive nonredundant protein database (SwissProt 2011_07) using MASCOT programs via the Internet.

Analysis of protein thiols with biotin–HPDP

The numbers of free and total protein cysteines were determined according to Baty and co-workers [28] with minor modifications. Briefly, HGF protein extracts were obtained in lysis buffer supplemented with 2 mM NEM. Cell lysates were treated for 15 min with 1 mM DTT and mixed with 2 volumes of 100% acetone. Proteins were allowed to precipitate for 30 min at -20°C , centrifuged at 10,000g for 10 min, at 4°C , and washed with 70% acetone and protein pellets were resuspended in 50 mM PBS (pH 7.4), supplemented with 100 μM biotin–HPDP. After 10-min incubation at room temperature, proteins were precipitated as described previously and resuspended with an equal volume of $2\times$ nonreducing Laemmli SDS–PAGE sample buffer. After SDS–PAGE separation on 12% (w/v) polyacrylamide gels, protein samples were electroblotted onto a PVDF membrane. After a 1-h saturation step in 5% (w/v) nonfat dry milk in PBST (10 mM Na phosphate (pH 7.2), 0.9% (w/v) NaCl, 0.1% (v/v) Tween 20), membranes were washed three times with PBST for 5 min each and the linked biotin–HPDP was probed by a 2-h incubation with 5% milk/PBST containing streptavidin–HRP at 1:5000 dilution. After three washes with PBST for 5 min each, protein bands were visualized by ECL detection.

Measurement of intracellular glutathione

GSH was measured after derivatization with mBrB. Control and smoke-treated HGFs were washed twice with PBS and harvested by trypsinization. Cell lysates were obtained in ice-cold lysis buffer supplemented with protease inhibitors as described above. Aliquots of samples were given 0.5 mM mBrB (final concentration) and incubated for 10 min at room temperature, in the dark; samples were then acidified with 3% (v/v, final concentration) trichloroacetic acid (TCA) and injected into a Sephasil C18 HPLC column. Glutathione disulfide (GSSG) and glutathione linked to protein cysteine residues, i.e., S-glutathionylated proteins (PSSG) were measured in other aliquots of cell lysates after addition of 0.5 mM (final concentration) NEM and, after 5 min, acidification with 4% (w/v, final concentration) TCA. GSSG was detected in the supernatant and PSSG in the protein pellets after DTT reduction and mBrB conjugation as previously reported [29]. Derivatized thiols were analyzed by fluorescence detection (excitation 380 nm; emission 480 nm) and quantified using authentic GSH similarly derivatized with mBrB using a Hewlett Packard HPLC Series 1100 as previously reported [29].

Preparation of GSH–acrolein (GSH–ACR) and GSH–crotonaldehyde (GSH–CRO) adducts and electrospray ionization mass spectrometry (ESI–MS) direct infusion analysis

Stock solutions of GSH–ACR and GSH–CRO were obtained by incubating for 24 h at 37°C GSH (final concentration 20 mM) in the presence of 2 mM either acrolein or crotonaldehyde in 1 mM phosphate buffer (pH 7.4) and then stored at 4°C until use. Sample aliquots were directly analyzed by HPLC for the determination of hydroxynonenal consumption, as previously described [30]: the reaction was quantitative as no residual aldehyde was determined. Therefore, samples (50 μl) were diluted 1:5 with $\text{H}_2\text{O}:\text{CH}_3\text{OH}:\text{EFBA}$ 90:10:0.1 (v/v/v) and analyzed by ESI–MS (direct infusion), using a TSQ Quantum triple-quadrupole mass spectrometer (ThermoFinnigan Italia, Milan, Italy). ESI interface parameters (positive-ion mode) were set as follows: middle position, capillary temperature 270°C , spray voltage 4.5 kV. Nitrogen was used as nebulizing gas at the following pressures: sheath gas 30 psi, auxiliary gas 5 a.u. MS conditions and tuning were performed by mixing through a T connection the water-diluted stock solutions of analytes (flow rate 10 $\mu\text{l}/\text{min}$), with the mobile phase maintained at a flow rate of 0.2 ml/min: the intensity of the $[\text{M} + \text{H}]^+$ ions was monitored and adjusted to the maximum using

Quantum Tune Master software. The Michael adducts of GSH with acrolein and crotonaldehyde were detected at m/z 364.0 and m/z 378.0, respectively.

GSH–acrolein and GSH–crotonaldehyde adduct analysis by LC–MS/MS

Method development

LC–MS/MS analysis and separation of the adducts were done using a ThermoFinnigan Surveyor LC system equipped with a quaternary pump, a Surveyor UV–Vis Diode Array Programmable Detector 6000 LP, a Surveyor autosampler, and a vacuum degasser and connected to a TSQ Quantum triple-quadrupole mass spectrometer (ThermoFinnigan Italia). Chromatographic separations were performed at 25°C by a Phenomenex Sinergy polar–RP column ($150\times 2\text{-mm}$ i.d.; particle size 4 μm ; Chemtek Analytica, Anzola Emilia, Italy) protected by a polar–RP guard column ($4\times 2\text{-mm}$ i.d.; 4 μm) kept at 25°C . The mass spectrometer was equipped with an ESI interface, which was operated in positive-ion mode and controlled by Xcalibur software (version 1.4).

Separations (injection volume 10 μl) were performed at a flow rate of 0.2 ml/min by gradient elution from 100% $\text{H}_2\text{O}:\text{CH}_3\text{OH}:\text{HFBA}$ (A) (9:1:0.01, v/v/v) to 60% methanol (B) in 16 min, followed by 5 min for the reequilibration of the system to the initial conditions. The samples rack was kept at 4°C . ESI interface parameters (positive-ion mode) were set as follows: middle position, capillary temperature 270°C , spray voltage 4.5 kV. Nitrogen was used as nebulizing gas at the following pressures: sheath gas 30 psi, auxiliary gas 5 a.u.

Ionization efficiency in the presence of the mobile-phase modifiers was monitored in multiple-reaction monitoring (MRM) mode at 2.00 kV multiplier voltage; the following MRM transitions of $[\text{M} + \text{H}]^+$ precursor ions \rightarrow product ions were selected for each analyte and internal standard and the relative collision energies were optimized by the Quantum Tune Master software:

- GSH–acrolein, m/z 364.0 \rightarrow m/z 216.9 (collision energy at 16);
- GSH–crotonaldehyde, m/z 378.0 \rightarrow m/z 128.0 + m/z 231.0 (collision energy at 18);
- TH (internal standard), m/z 319.2 \rightarrow m/z 156.2 + m/z 301.2 (collision energy at 25).

For quantitative analysis the instrument parameters were optimized as follows: argon gas pressure in collision Q2, 1.5 mbar; resolution (FWHM), 0.70 m/z at Q1 and Q3; scan width for all MRM channels, 1 m/z ; scan rate (dwell time), 0.2 s/scan. Data processing was performed using Xcalibur version 2.0 software.

Working solutions of GSH–ACR and GSH–CRO were obtained by dilution in PBS of the corresponding stock solutions. Calibration samples for GSH–ACR and GSH–CRO adducts were prepared by spiking blank supernatants or cell lysates with each working solution, to provide the following final concentrations: 0.05, 0.1, 1, 5, 10, or 20 μM . Aliquots of 90 μl were then mixed with 10 μl of a 200 μM internal standard solution in mobile phase (5 μM final concentration). Samples were given 100 μl of 700 mM perchloric acid (aqueous solution) and subsequently centrifuged at 20,000g for 10 min. The supernatant was diluted 1:2 with $\text{H}_2\text{O}:\text{CH}_3\text{OH}:\text{HFBA}$ 90:10:0.1 (v/v/v) and filtered through 0.45- μm nylon Millex–HV filters (Millipore) before injection. Standard curves for the analytes constructed on different working days showed good linearity over the entire calibration ranges, with coefficients of correlation (r^2) greater than 0.998.

Method application

Ninety-microliter aliquots of HGF cell lysates and of cell supernatants were mixed with 10 μl of a 200 μM internal standard solution in mobile phase (5 μM final concentration), treated as described above, and injected into the LC–MS/MS system for quantization of GSH–ACR and GSH–CRO adducts. Data were calculated as nmol/ml and expressed as $\text{nmol}/10^6$ cells.

Statistical analysis

Quantitative data are expressed as means \pm SD of three independent experiments or as data \pm SEM. Differences between means were evaluated using one-way analysis of variance with Tukey's multiple comparison posttest unless otherwise indicated. A value of $p < 0.05$ was considered statistically significant.

Results

Intracellular reactive oxygen species generation

We quantified the level of intracellular oxidative stress induced by cigarette smoke by measuring ROS formation in HGFs using the oxidation-sensitive nonfluorescent DCFH-DA. The intracellular DCF

fluorescence can be used as an index to quantify ROS production (and overall oxidative stress) in cells, being an indicator of generalized oxidative stress rather than of any particular reactive species (e.g., it is not a direct assay for H_2O_2 or other specific ROS) [31]. Whole (mainstream) cigarette smoke induces intracellular oxidative stress: Fig. 1A shows that exposure of HGFs to whole cigarette smoke produced a dose-dependent (i.e., puff-dependent) increase in intracellular ROS generation.

Analysis of cell viability and cell morphology

The viability of cultured HGF, determined by trypan blue exclusion analysis after exposure to 0.5–12 cigarette puffs (Fig. 1B), was dose-dependently decreased by treatment with whole cigarette smoke, ranging from $97.7 \pm 2.7\%$ for cells exposed to 0.5 cigarette puff to $88 \pm 9\%$,

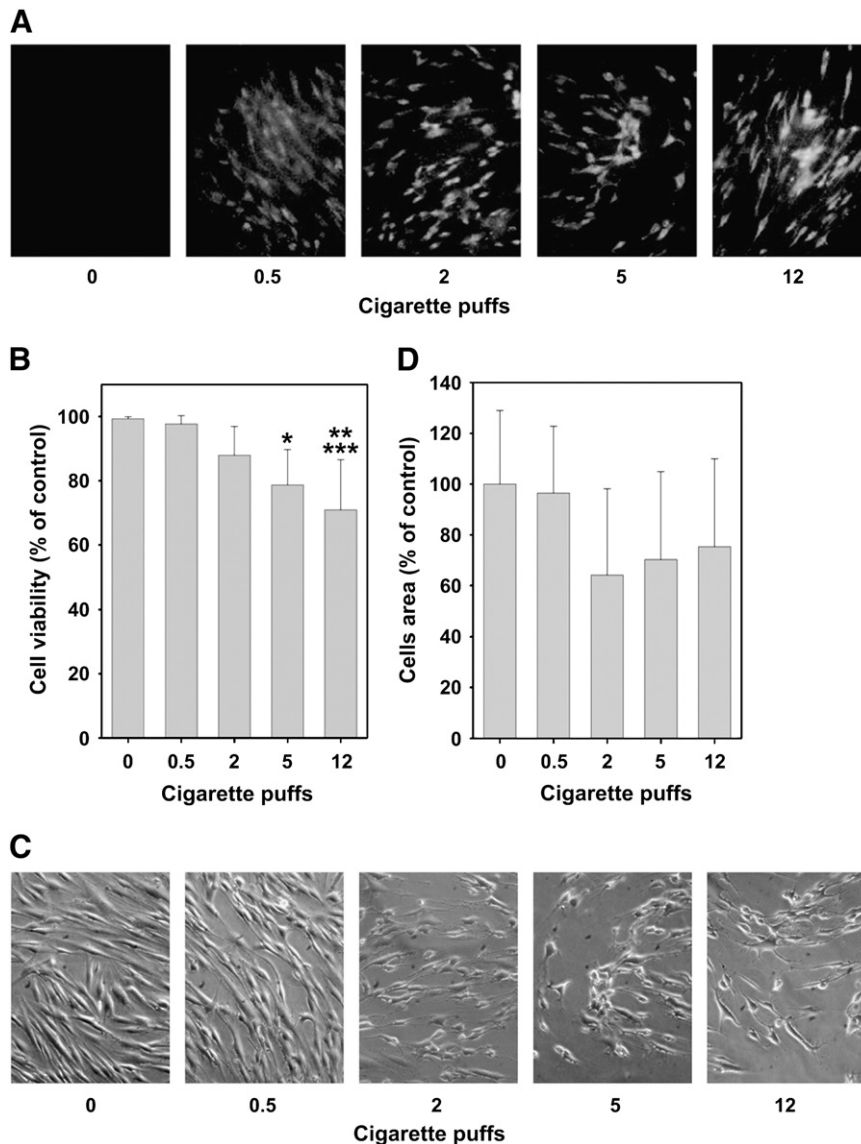


Fig. 1. Intracellular ROS formation, loss of HGF viability, and cellular morphology. (A) Representative images of the increase in DCF fluorescence (480 nm excitation, 527 nm emission) induced by exposure of cultured HGFs to 0, 0.5, 2, 5, and 12 cigarette puffs. Exposure of HGFs to whole cigarette smoke produced a dose-dependent (i.e., puff-dependent) increase in intracellular ROS generation. All exposed cells revealed a fairly uniform distribution of the fluorescence, indicative of the spreading of ROS production within the cells. (B) Loss of cell viability with increasing puffs of cigarette smoke. Cultured HGFs were exposed to 0, 0.5, 2, 5, and 12 cigarette puffs and cell viability was evaluated by the trypan blue exclusion method. Values are expressed as the means \pm SD of three independent experiments ($n = 3$) and $*p < 0.01$ vs control, $**p < 0.001$ vs control, $***p < 0.05$ vs 0.5 puffs as evaluated by the Student–Neumann–Keuls test. (C) Shrinkage of HGFs exposed to increasing puffs of cigarette smoke. HGFs were exposed to 0, 0.5, 2, 5, and 12 cigarette puffs and their morphology was examined under a phase-contrast microscope. Unexposed HGFs (controls) showed typical morphology, consisting in a population of spindle-shaped or stellate cells. Aberrations in the cellular morphology were observed in the cells exposed to 2–12 cigarette puffs, which showed a smaller size, a less elongated shape, and a more globular cell body. By contrast, exposure to 0.5 puff had no significant effect on the cellular morphology. (D) For each dose of cigarette puffs, the area of about 100 single cells was measured and plotted with respect to puff number. Results are expressed as the means \pm SD of three independent experiments ($n = 3$) and $p < 0.05$ vs control.

78.7 ± 11, and 70.9 ± 15% for cells exposed to 2, 5, and 12 cigarette puffs, respectively. The effect of mainstream cigarette smoke on the morphology of HGFs was assessed by phase-contrast microscopy. Unexposed HGFs (control) showed regular shape. Aberrations in the cellular morphology were observed in the cells exposed to 2–12 cigarette puffs, whereas exposure to 0.5 puff had no significant effect on the cellular morphology (Fig. 1C). Exposure of HGFs to 2–12 puffs of whole cigarette smoke caused cellular shrinkage and contraction, therefore impairing cellular integrity (Fig. 1D).

Analysis of protein carbonylation

Protein carbonylation, a stable index of irreversible oxidation, can be assayed by immunochemical methods after formation of the DNP adduct [24,25]. Immunocytochemical techniques were used to determine the formation of carbonyl groups in HGFs exposed to 0.5–12 cigarette puffs (Fig. 2A). The fixed cells were incubated with DNPH solution, then with anti-dinitrophenyl-KLH antibody, and finally with a goat anti-rabbit FITC-conjugated secondary antibody. In control HGFs and in fibroblasts exposed to 0.5 cigarette puffs no carbonyl-specific staining was observed by fluorescence microscopy, whereas HGFs exposed to 2–12 cigarette puffs showed a diffuse DNP immunoreactivity throughout the cytoplasm, indicative of protein carbonylation. Distribution of smoke-induced protein carbonylation in whole-cell lysates was analyzed by Western immunoblotting. As shown in Fig. 2B, exposure of HGFs to 0.5–12 cigarette puffs induced a marked, dose-dependent increase in protein carbonylation. Fig. 2B demonstrates that proteins of HGFs exposed to mainstream cigarette smoke are highly carbonylated in comparison to those extracted from untreated cells. Several carbonylated proteins were

identified in HGFs exposed to 5 cigarette puffs by means of redox proteomics [32], using the MASCOT search engine and human proteins available in the SwissProt database (Fig. 2D and Table 1). Nine of the 21 highly carbonylated proteins we identified in HGFs exposed to cigarette smoke were slightly or moderately carbonylated also in the control, i.e., HGFs not exposed to cigarette smoke (Fig. 2C).

Analysis of thiol redox status

Fig. 3 shows the effects of whole-smoke exposure on the reversibly oxidized thiol protein profiles of HGFs. A small percentage of protein thiols were already reversibly oxidized in untreated cells and no significant difference in thiol protein oxidation was observed after HGF exposure to 0.5 puff. Clear changes were observed in the pattern of oxidized protein thiols after HGF exposure to 2–12 puffs. All of the oxidized thiol proteins detected in untreated cells and in HGF exposed to 0.5 puff became more oxidized and a number of new bands were detectable after HGF exposure to 2–12 puffs, suggesting a reversible oxidation of protein thiols in response to smoke-induced oxidative stress.

Exposure of various cell types to cigarette smoke causes rapid depletion of intracellular GSH, which often parallels cell toxicity [33]. We determined the amount of total glutathione (tGSH = GSH + 2GSSG + PSSG) in HGFs exposed to cigarette smoke by a validated HPLC method [34] (Fig. 4). Cigarette smoke markedly depleted total intracellular levels of glutathione.

Under oxidative stress, GSH can oxidize to its disulfide forms, GSSG and PSSG. We therefore examined the cellular levels of the various forms of glutathione to ascertain possible alterations in the levels of GSH, GSSG, and/or PSSG contributing to the decrease in tGSH

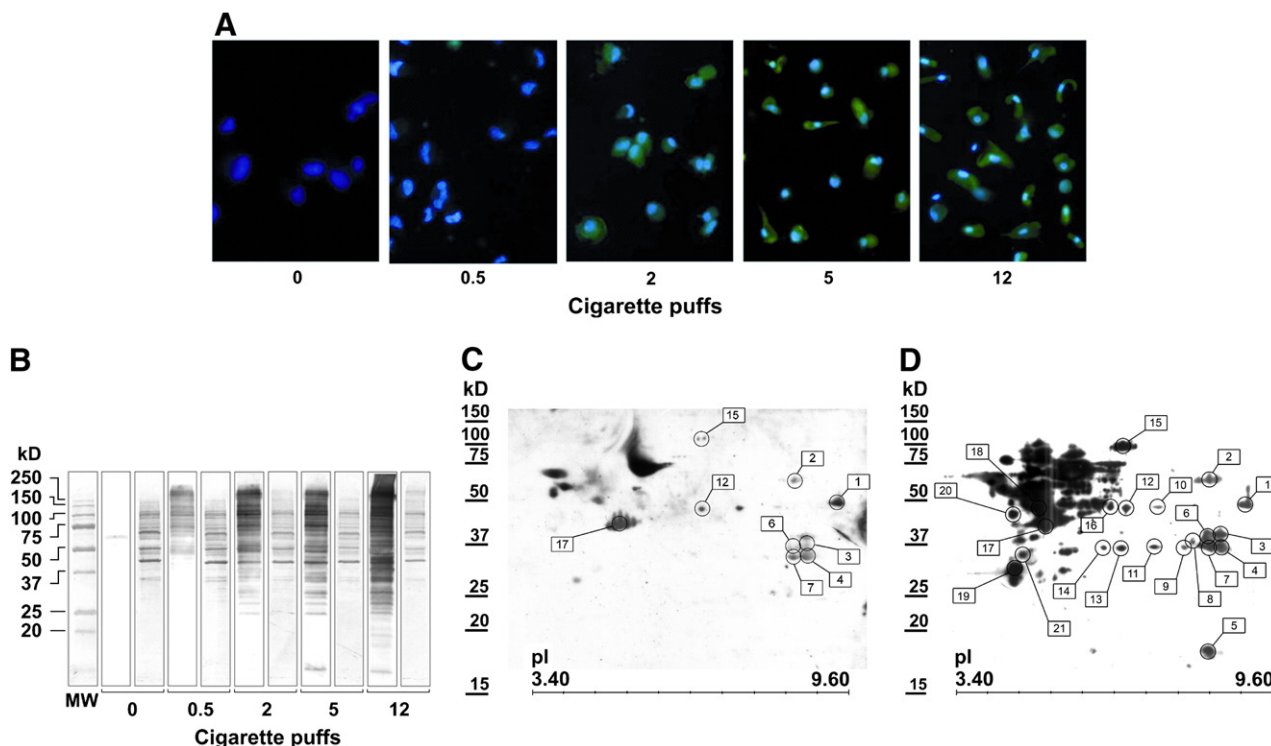


Fig. 2. Cigarette smoke-induced formation of protein carbonyls in HGFs. (A) Cigarette smoke-induced protein carbonylation in HGFs exposed to 0, 0.5, 2, 5, and 12 cigarette puffs was assessed by an immunocytochemical DNPH assay as described under Materials and methods and observed by fluorescence microscopy. Representative microphotographs of two independent experiments are shown. To see this illustration in color the reader is referred to the Web version of this article at <http://ees.elsevier.com/frbm>. (B) Protein carbonylation in whole-cell lysates from HGFs exposed to 0, 0.5, 2, 5, and 12 cigarette puffs was detected using a Western blot assay including carbonyl derivatization with DNPH as described under Materials and methods. A representative Western blot of the protein carbonylation pattern (lane on the left in each pair) and the corresponding amido black protein staining (lane on the right in each pair) are shown. Lane 0 shows the protein carbonyl pattern of HGFs incubated in PBS alone (control). MW, molecular weight protein standards. Each pair shows a single representative experiment of three separate experiments. No immunostaining was observed in parallel experiments in which either the protein samples were treated with NaBH₄ or the primary antibody to DNP was omitted (not shown). (C, D) Representative 2D immunoblots corresponding to the detection of carbonylated proteins in homogenates of (C) control HGFs and (D) HGFs exposed to 5 cigarette puffs. Identified proteins are listed in Table 1.

Table 1
Identified carbonylated proteins in HGFs exposed to five cigarette puffs.

Spot	Identification	Mass (Da)	pI	MASCOT score	Number of hits		Coverage
					Matched	Total	
1	Elongation factor 1- α 1	50,451	9.10	70	9	12	26
2	Pyruvate kinase isozyme M1/M2	58,470	7.96	157	18	23	42
3	Fructose-bisphosphate aldolase A	39,851	8.40	97	9	16	32
4	Glyceraldehyde-3-phosphate dehydrogenase	36,201	8.57	58	7	26	23
5	Cofilin 1	18,719	8.22	66	6	7	42
6	Annexin A2	38,808	7.57	105	11	14	30
7	Glyceraldehyde-3-phosphate dehydrogenase	36,201	8.57	59	8	12	20
8	Annexin A2	38,808	7.57	92	14	20	39
9	Glyceraldehyde-3-phosphate dehydrogenase	36,201	8.57	70	10	15	26
10	α -Enolase	47,481	7.00	58	5	5	16
11	Annexin A1	38,918	6.57	70	8	12	22
12	α -Enolase	47,481	7.00	132	13	14	41
13	Annexin A1	38,918	6.57	101	12	18	35
14	Annexin A1	38,918	6.57	72	7	8	19
15	Elongation factor 2	96,246	6.41	155	18	21	23
16	α -Enolase	47,481	7.00	80	10	17	24
17	Actin, cytoplasmic isoform 1, 2	42,052	5.29	86	10	18	36
18	Actin, cytoplasmic isoform 1, 2	42,052	5.29	100	8	15	27
19	Tropomyosin α -4 chain	28,619	4.67	77	13	28	37
20	Ribonuclease inhibitor	51,766	4.71	75	9	22	30
21	Annexin A5	35,971	4.94	170	27	37	48
21	Annexin A5	35,971	4.94	170	27	37	48

Spot numbers are the same as those used to identify proteins shown in the gel provided in Fig. 2C. pI, isoelectric point. Database: SwissProt. Protein scores are all biologically significant ($p < 0.05$).

levels. The marked decrease in intracellular GSH levels we measured in all HGFs exposed to 0.5–12 puffs, with HGFs exposed to 12 puffs exhibiting the largest decline in GSH level (Fig. 5A), was only minimally compensated for by oxidation of GSH to GSSG (Fig. 5B) and by little increases in PSSG levels (Figs. 5C and D). In addition, the increases in GSSG and PSSG were even scarcer in HGF exposed to 12 puffs (Figs. 5B–D). As a whole, these data indicate that exposure to whole cigarette smoke notably decreases GSH levels and, concurrently, very moderately increases GSSG and PSSG levels, in HGF.

Determination of GSH- α,β -unsaturated aldehyde adducts

We therefore hypothesized that the decrease in intracellular GSH (and, consequently, that of tGSH) could be induced by export of GSH to the extracellular environment as GSH adducts with α,β -unsaturated aldehydes, which are contained in high concentrations in whole cigarette smoke. To test this possibility, we developed a new analytical

methodology for the detection and quantification of GSH adducts with acrolein and crotonaldehyde (GSH-ACR and GSH-CRO, respectively), two of the major highly reactive aldehydes in tobacco smoke. First, we prepared the adducts by incubation of GSH with the aldehydes. Fig. 6 shows the CID spectra of GSH-ACR (Fig. 6A) and GSH-CRO (Fig. 6B), obtained by collision of the corresponding $[M+H]^+$ at m/z 364.0 and 378.0, respectively (infusion experiments), at a collision energy of 20 eV. The most abundant and stable product ions were chosen for setup using an MRM transitions-based LC-MS/MS method (quantitative analysis). The method was validated as described in the Supplementary Material and then applied to monitor the intracellular formation of GSH-ACR adducts and GSH-CRO adducts over a 2-h time course, in HGFs exposed to 0.5–12 puffs, as well as their extracellular export, determining such GSH-aldehyde adducts in the extracellular medium. As an example, Fig. 7 reports the LC-MS/MS profiles of intracellular medium, relative to human HGFs exposed to 12 cigarette

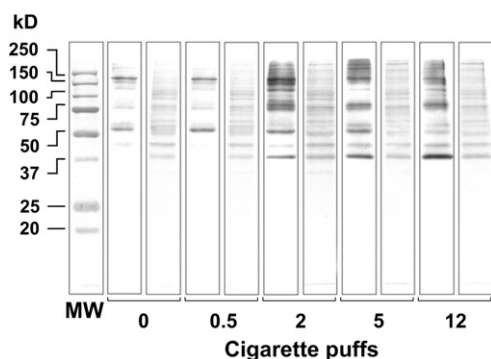


Fig. 3. Reversibly oxidized protein thiols. The increase in reversibly oxidized protein –SH residues in whole-cell lysates from HGFs exposed to 0, 0.5, 2, 5, and 12 cigarette puffs was assessed by the use of biotin-HPDP and Western blotting probed with HRP-conjugated streptavidin, as described under Materials and methods. In each pair of lanes, the lane on the left shows the Western blot developed with ECL, whereas the lane on the right shows the corresponding PVDF membrane stained for proteins with amido black. MW, molecular weight protein standard. Each pair shows a single representative experiment of three separate experiments.

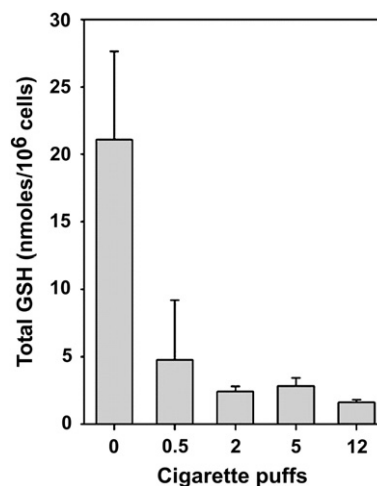


Fig. 4. Cigarette smoke-induced depletion of total glutathione in HGFs. Depletion of total glutathione (GSH + 2GSSG + PSSG) in whole-cell lysates from HGFs exposed to 0, 0.5, 2, 5, and 12 cigarette puffs was assessed by an HPLC method as described under Materials and methods. Results are expressed as the means \pm SD of three replicate measurements ($n = 3$) and $p < 0.05$ vs control.

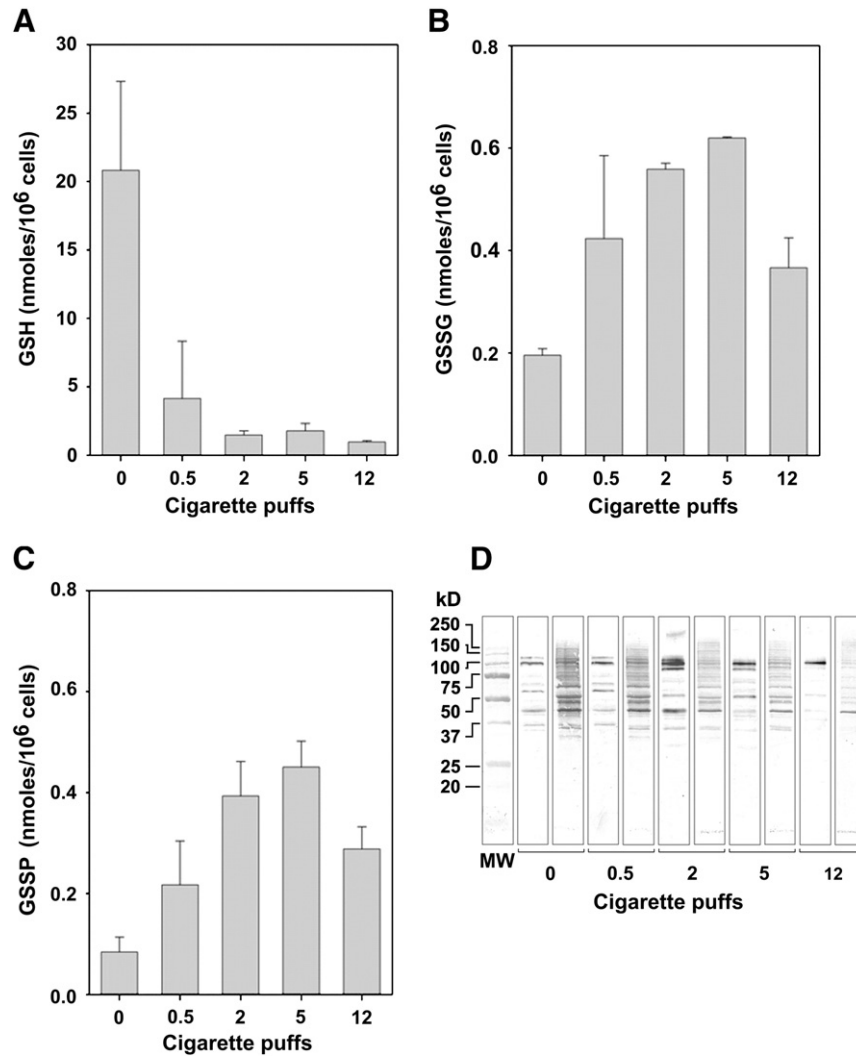


Fig. 5. Effects of cigarette smoke on the levels of GSH, GSSG, and protein S-glutathionylation in HGFs. Changes in (A) GSH and (B) GSSG levels in whole-cell lysates from HGFs exposed to 0, 0.5, 2, 5, and 12 cigarette puffs were assessed by an HPLC method as described under Materials and methods. Results are expressed as the means \pm SD of three replicate measurements ($n=3$) and $p<0.05$ vs control. (C) Protein S-glutathionylation in whole-cell lysates from HGFs exposed to 0, 0.5, 2, 5, and 12 cigarette puffs was quantified by reversed-phase HPLC coupled with fluorometric detection after derivatization of protein-bound GSH with mBrB. Results are expressed as the means \pm SD of three replicate measurements ($n=3$) and $p<0.05$ vs control. (D) Western blot analysis of protein S-glutathionylation in whole-cell lysates from HGFs exposed to 0, 0.5, 2, 5, and 12 cigarette puffs was performed using anti-GSH monoclonal antibody as described under Materials and methods. In each pair of lanes, the lane on the left shows the Western blot developed with ECL, whereas the lane on the right shows the corresponding PVDF membrane stained for proteins with amido black. MW, molecular weight protein standards. Each pair shows a single representative experiment of three separate experiments.

puffs, in which the typical MRM peaks relative to the internal standard (Fig. 7A), GSH-ACR (Fig. 7B), and GSH-CRO (Fig. 7C) are easily detectable (although with different intensities) at the expected retention times.

The results of the quantitative analysis of both GSH-aldehyde adducts at various observation times and conditions are summarized in Figs. 8 and 9. Although at the first observation time (0 min) no significant differences were found between HGFs exposed to 2 and 5 puffs,

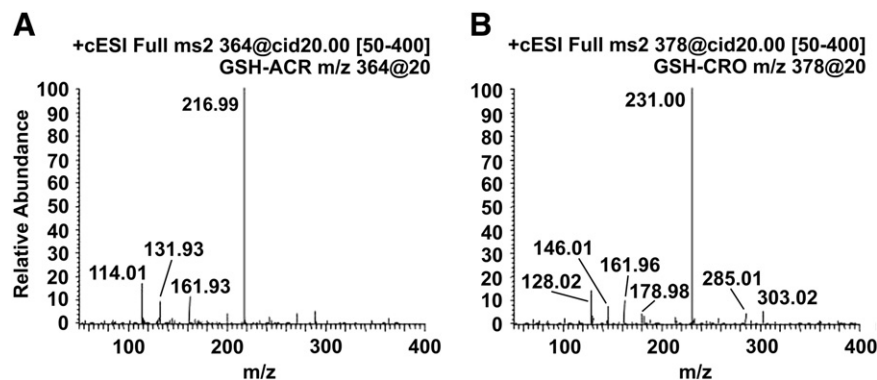


Fig. 6. Positive ESI-MS/MS spectra (direct infusion experiments) of (A) GSH-ACR and (B) GSH-CRO adducts, acquired at 20 V collision energy.

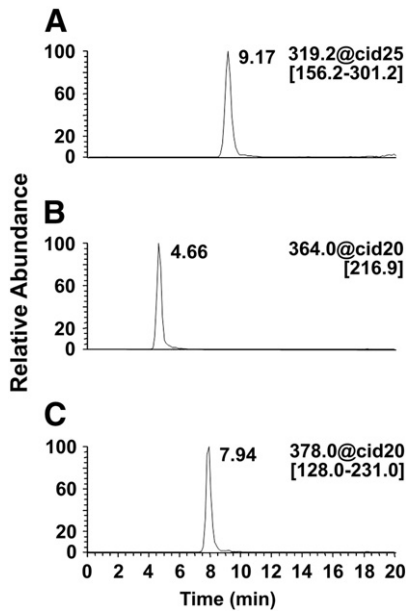


Fig. 7. LC-ESI-MS/MS analysis profile (MRM mode) of intracellular medium relative to HGFs exposed to 12 cigarette puffs: (A) internal standard, (B) GSH-ACR, (C) GSH-CRO.

cigarette smoke led to a clear dose-dependent intracellular formation of both the adducts (Figs. 8A and 9A). The intracellular levels of GSH-ACR and GSH-CRO significantly declined already at 30 min after cigarette smoke exposure and, consistently, they dose-dependently increased in the extracellular medium (Figs. 8B and 9B) to indicate an export of both adducts from the cell. At the subsequent observation times, the increase in the extracellular levels of GSH-aldehyde adducts was even more pronounced and was paralleled by an almost complete intracellular disappearance of both adducts. Table 2 shows the cumulative sum of intra- and extracellular adduct levels, and these data indicate that formation of ACR is far greater than that of CRO. In addition, by considering the total amount of GSH consumed for the formation of intra- and extracellular GSH-ACR and GSH-CRO (2.097, 4.019, 5.174, and 6.040 nmol/ 10^6 cells at 0.5, 2, 5, and 12 puffs, respectively), it is evident that GSH depletion reported in Fig. 4 is due only in part to detoxification of cytotoxic aldehydes.

Discussion

Cigarette smoking can directly affect gingival tissues/cells because the oral cavity is the first area exposed to the smoke. Several studies

have demonstrated deteriorating effects of smoking on oral tissues [4,5,35]. Gingival fibroblasts, the predominant cell type inhabiting the gingival connective tissue, play a critical role in remodeling and maintaining gingival structures and extracellular matrix [36] and in tissue repair and wound healing [37] through their adhesion, migration, growth, proliferation, and differentiation, as well as production of extracellular matrix. However, exposure to cigarette smoke can hamper fibroblast function and consequently that of gingival tissue. Secondary to bacterial plaque, cigarette smoking is a major risk factor for periodontal disease and even promotes its development [38,39]. However, the exact mechanisms leading to smoking-related oral disease processes still need to be fully understood. In particular, the effect of whole cigarette smoke on gingival fibroblasts has yet to be elucidated.

In this study, we observed that exposure to cigarette smoke exerted a rapid and lethal effect on HGFs (Fig. 1B) as well as inducing aberrations in their cellular morphology (Figs. 1C and D). No apoptotic cellular bodies were evidenced under the phase-contrast microscopy, and DAPI staining did not reveal the occurrence of nuclear condensation, DNA fragmentation, or perinuclear apoptotic bodies. Therefore, we think it is highly unlikely that the reduction in HGF viability after exposure to cigarette smoke was due to apoptosis. Because of the short duration of cigarette smoke necessary until these effects become manifest, we tend to exclude complex signal transduction pathways (via transcription and/or translation) from being involved in these processes. Increase in intracellular ROS (Fig. 1A) and carbonylation of proteins (Fig. 2), including some cytoskeletal proteins and the actin-depolymerizing factor cofilin-1 (Table 1), may be one, although not the only, possible explanation, because such a rapid death can result from modifications and destruction of protein structures and/or impairment of metabolic pathways. The fibroblast cytoskeleton plays a key role in basic cell functions such as motility, adhesion, and division. Actin filaments, in particular, play central and fundamental roles in the shaping of cells, the maintenance of cell integrity, and the stability of cytoskeletal interaction, as well as cell substrate adhesion. Cellular shrinkage and rounding depend on perturbation of filamentous actin (F-actin). Carbonylation of actin and some actin-binding/remodeling proteins such as cofilin-1, which promotes cytoskeletal dynamics by mediating severing and depolymerization of actin filaments in mammalian nonmuscle cells, playing an important role in cytokinesis, cell motility, and morphogenesis in mammals [40]; elongation factor 1- α , the second most abundant protein in eukaryotic cells after actin, which has been shown to associate with and reorganize F-actin, inducing filament bundling [41]; and annexin A2, which has a role as an actin nucleator on phosphatidylinositol 4,5-bisphosphate-enriched

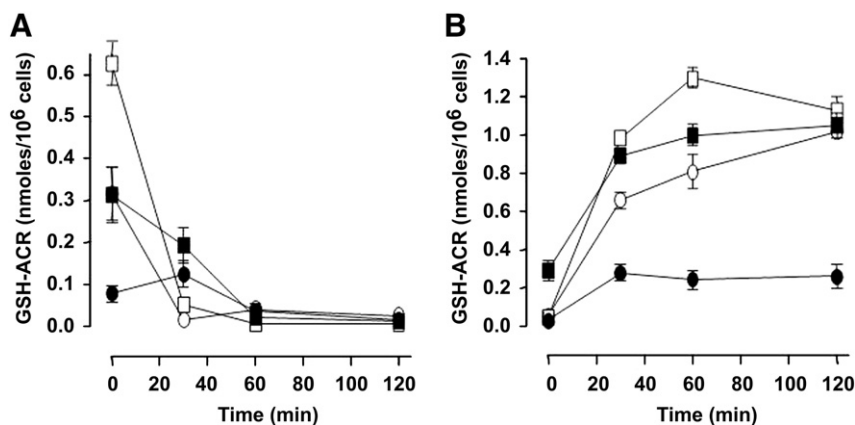


Fig. 8. LC-ESI-MS/MS quantitative analysis of (A) intracellular and (B) extracellular GSH-ACR adducts after HGF exposure to 0.5 (●), 2 (○), 5 (■), and 12 (□) cigarette puffs. Values are expressed as data \pm SD of three independent experiments (duplicate injection) ($n = 3$). All data were statistically different (versus time 0) except for those relative to 0.5 cigarette puff (at least $p < 0.05$).

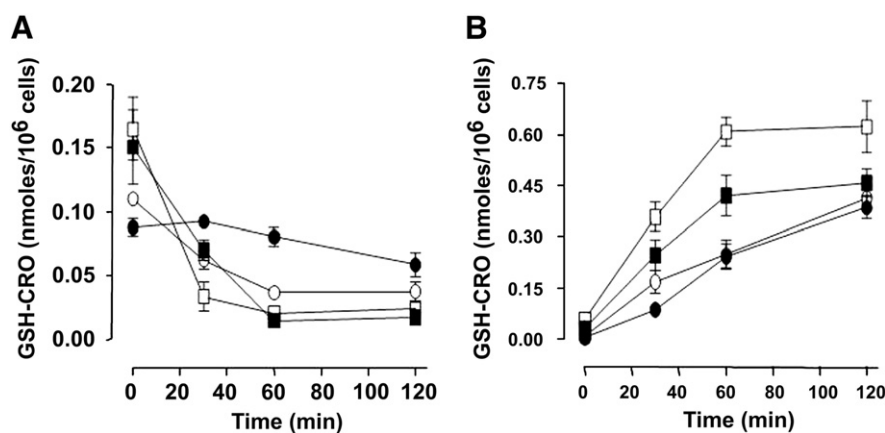


Fig. 9. LC-ESI-MS/MS quantitative analysis of (A) intracellular and (B) extracellular GSH-CRO adducts after HGF exposure to 0.5 (●), 2 (○), 5 (■), and 12 (□) cigarette puffs. Values are expressed as data \pm SD of three independent experiments (duplicate injection) ($n = 3$). All data were statistically different (versus time 0) (at least $p < 0.05$).

cell membranes [42] and whose tyrosine phosphorylation is an important event in triggering Rho/ROCK-dependent and actin-mediated changes in cell morphology associated with the control of cell adhesion [43], can impair the fibroblast actin-based cytoskeleton. In particular, functional studies performed *in vitro* revealed significant inhibition of polymerization rate and extent, progressive disruption of actin filaments [44,45], and reduction in the activation of the myosin ATPase activity [45] for carbonylated actin compared to control actin. Enhancement of actin carbonylation, causing the disruption of the actin cytoskeleton and the loss of the barrier function, was found in cultured human colonic cells after exposure to hypochlorous acid or hydrogen peroxide [46,47]. Marked actin carbonylation was also seen in inflamed colonic mucosa from patients affected with inflammatory bowel disease, suggesting that oxidant-induced cytoskeletal disruption is required for tissue injury, mucosal disruption, and inflammatory bowel disease flare up [48]. Cytoskeleton disorganization was also observed in human colon cancer cells after actin carbonylation owing to acrolein adduction [49]. Furthermore, carbonylation of actin and tropomyosin is largely increased in failing human hearts and is inversely correlated with left ventricular ejection fraction, thus probably contributing to the contractile impairment evident in end-stage heart failure [50]. Therefore, irreversible oxidative modification of actin and some actin-associated proteins of gingival fibroblasts would be expected to alter their locomotion and phagocytosis of collagen, which are actin-dependent functions important for physiological tissue remodeling and periodontal wound repair. The direct cytopathic effect of cigarette smoke on HGF supports the hypothesis that cigarette smoke is a

great risk factor in the development and progression of periodontal disease, impairing the ability of gingival fibroblasts to maintain the integrity of the oral connective tissue or to repair it during periodontal destruction or wound healing. Reduced cell viability, modified cell morphology, disruption of the microtubule network, and oxidative damage of tubulin, detected as increased carbonyl content, were recently observed in human lung epithelial (A549) cells and noncarcinoma human lung alveolar epithelium (L132) cells exposed to aqueous extract of cigarette smoke [51]. Furthermore, some of the carbonylated proteins detected in cigarette smoke-exposed HGFs are involved in energy metabolism. Therefore, their oxidative modification may impair their function and, consequently, the HGF energy production. α -Enolase is a glycolytic enzyme that hydrolyzes 2-phosphoglycerate to phosphoenol pyruvate in glycolysis, and impairment of this enzyme can greatly affect ATP production. Glyceraldehyde-3-phosphate dehydrogenase (GAPDH) is another glycolytic enzyme that catalyzes the oxidation of glyceraldehyde 3-phosphate to 1,3-bisphosphoglycerate and NADH. As a result, the increased carbonylation of GAPDH and α -enolase could lead to impaired glycolytic function and decreased ATP production. Fructose-1,6-bisphosphate aldolase cleaves fructose 1,6-bisphosphate into dihydroxyacetone phosphate and glyceraldehyde 3-phosphate in glycolysis. Its impairment can cause increased levels of fructose 1,6-bisphosphate, inhibition of complete glycolysis, and ATP depletion.

As shown in Fig. 3, the increase in total reversibly oxidized protein thiols parallels the increase in cigarette puffs, suggesting a dose-dependent oxidation of protein cysteine residues in response to smoke. Cellular thiol redox status is critical for a variety of biological processes including transcriptional activation of various genes, regulation of cell proliferation, inflammation, and apoptosis. Thiols, particularly GSH, are also critical for cellular antioxidant defenses, including protecting cells from oxidant injury and inflammation. When cells are exposed to oxidizing conditions, GSH can be oxidized to GSSG and/or be reversibly bound to protein cysteine residues, by a process called S-glutathionylation, forming PSSG [52]. Cellular GSH concentration, by modulating the redox intracellular environment, also plays a key role in regulating cellular signaling events resulting from the action of redox-sensitive proteins [53]. As a nucleophile, GSH also functions as a scavenger, which conjugates with reactive intermediates derived from exogenous agents. Because of this dual function in shielding against the attacks of endogenous and exogenous toxic species, GSH is essential in maintaining normal biochemical and physiological functions in tissues, and the cellular depletion of GSH can lead to significant cell/tissue damage [31].

In this study, we demonstrate for the first time that total glutathione (GSH + 2GSSG + PSSG) decreased dramatically within HGF after

Table 2

Sum of intra- and extracellular GSH-ACR and GSH-CRO levels after 0.5, 2, 5, and 12 cigarette puffs.

	0.5 cp	2 cp	5 cp	12 cp
GSH-ACR (nmol/10 ⁶ cells)				
0 min	0.107	0.369	0.603	0.674
30 min	0.402	0.672	1.082	1.036
60 min	0.277	0.849	1.021	1.302
120 min	0.274	1.043	1.06	1.136
Total	1.06	2.933	3.766	4.148
GSH-CRO (nmol/10 ⁶ cells)				
0 min	0.09	0.119	0.181	0.222
30 min	0.179	0.229	0.316	0.393
60 min	0.323	0.286	0.436	0.629
120 min	0.445	0.452	0.475	0.648
Total	1.037	1.086	1.408	1.892
GSH-ACR + GSH-CRO (GSH consumption) (nmol/10 ⁶ cells)	2.097	4.019	5.174	6.04

cp, cigarette puffs.

whole cigarette smoke exposure (Fig. 4), indicating that thiol depletion could be a mechanism for cigarette smoke-induced cytotoxicity. Intracellular GSH depletion by cigarette smoke might render the cells more vulnerable to oxidative/carbonyl stress in the oral cavity and might impair the reparative and regenerative potential of gingival tissues of smokers. Cellular loss of GSH, along with the reduced cellular vitality and carbonylation of some cytoskeletal proteins and cofilin-1, might also be correlated with the reduced reparative and regenerative activity of smoke-exposed gingival and periodontal tissues [35,54]. Cigarette smoke-induced depletion of intracellular GSH (Fig. 5A) was not accompanied by a corresponding formation of GSSG and PSSG (Figs. 5B–D). Subsequent experiments suggest that total GSH consumption is due to the export of GSH–acrolein (Fig. 8) and GSH–crotonaldehyde (Fig. 9) adducts. However, also in this case, the amount of the exported GSH–aldehyde adducts does not account for the marked depletion of intracellular GSH, not even if the amount of GSH reacted with acrolein and crotonaldehyde was added to the quantity of GSSG and PSSG formed after HGF exposure to cigarette smoke. The remaining depleted GSH could be due to reactions with some of the many other cigarette smoke-reactive components. As a major substrate for glutathione *S*-transferases (GSTs), GSH in cells could be largely depleted because of GST-mediated detoxification of xenobiotic compounds, including those present in cigarette smoke, in particular, high levels of various reactive aldehydes other than acrolein and crotonaldehyde, such as acetaldehyde, formaldehyde, and propanal. However, many reactive/electrophilic cigarette smoke components are also expected to react directly with GSH or other cellular thiols.

Our data would suggest that irreversible GSH alkylation by aldehydes or other reactive xenobiotics may be the most prominent mechanism by which whole cigarette smoke depletes cellular GSH in HGFs. However, multiple other free sulfhydryl groups and complex GSH pathways influence GSH homeostasis in vivo. For example, cigarette smoke-derived oxidants or aldehydes may inhibit several enzymes involved in GSH homeostasis, such as γ -glutamylcysteine synthetase, GSH reductase, and GSH peroxidase. Acrolein and crotonaldehyde themselves are well known to be toxic [e.g., 15,33]. Furthermore, GSH–acrolein and GSH–crotonaldehyde adducts have been shown to be toxic in humans and animal models [e.g., 55]. Hence, acrolein and crotonaldehyde reaction with GSH (as well as that of other unsaturated and saturated aldehydes) could represent a cellular defense mechanism, further illustrated by the observed increased endothelial dysfunction induced by exposure to tobacco smoke in mice lacking GST isoform P, which preferentially conjugates many of the small reactive carbonyls present in cigarette smoke, such as acrolein and crotonaldehyde [56].

Irreversible modification/depletion of GSH by reactive aldehydes renders it unavailable for the enzymatic reducing cycle system, which is normally activated after oxidative stress occurrence and the formation of GSSG. This exhaustion of the GSH pool could induce a chronic lack of antioxidant protection in HGFs. Persistent smokers might, in that case, inhale more ROS than can be scavenged by the residual antioxidants, resulting in increased vulnerability to oxidative stress of gingival/periodontal tissues.

Future research is needed both to better define the effects of smoke-derived oxidants and reactive carbonyl compounds on oral tissues and to determine the most efficacious strategies for generating significant antioxidant protection in the oral cavity. However, given some evidence of systemic oxidative stress in smokers [57,58], it is clear that the endogenous antioxidant response is inadequate to prevent the development of oxidative/carbonyl stress injury. In this respect, we have recently demonstrated that physiological (plasma) concentrations of glutathione, cysteine, and other antioxidants, i.e., ascorbic acid, methionine, and uric acid, which are strong reducing agents and potent antioxidants that act together in circulation, as well as the synthetic aminothiols *N*-acetylcysteine used at

pharmacological concentrations, are absolutely ineffective at preventing the cigarette smoke-induced thiol oxidation and carbonylation of human serum albumin (HSA) and plasma proteins on the whole. In contrast, human erythrocytes, by virtue of their rich and highly efficient antioxidant systems, coupled with their high blood concentration, were shown to be protective against cigarette smoke-induced oxidation (carbonylation and thiol oxidation) of both HSA and total human plasma proteins [59]. As a whole, the role of antioxidant supplementation in preventing smoke-associated diseases remains controversial [60–65], if not noxious, as shown in the case of high, long-term β -carotene supplementation in heavy smokers by several large, long-term intervention or epidemiological trials [66]. Anyway, a recent randomized controlled trial tested for 8 weeks the compliance, tolerability, and safety of two food-based antioxidant-rich diets in smokers: i.e., a comprehensive combination of antioxidant-rich foods (such as berries, nuts, spices, fruits, and vegetables) providing dietary antioxidants at levels that are similar to those only previously tested in randomized controlled trials using pharmacological doses of antioxidant supplements and a kiwi fruit diet, in which participants consumed three kiwi fruits, which are a rich source of vitamin C, per day [67]. This trial demonstrated the safety of both diets as no potentially harmful or pro-oxidative effects were observed and that the antioxidant-rich diet was particularly effective in terms of increasing plasma antioxidants. Future studies are needed to explore the impact of such dietary intervention strategies on the risk of chronic diseases related to oxidative stress, also in smokers.

Caution should be exercised in extrapolating the results of this study to in vivo conditions. However, the results of this research might lay the foundation for the effective use of drug-based strategies for ablating exposure to reactive carbonyl compounds as a tool to prevent, or reduce, smoke-related oral tissue damage, provided that the best “antioxidant” would be to give up smoking. α,β -Unsaturated and, probably, saturated aldehydes could therefore be potential pharmacologic targets for intervention strategies against smoking-induced tissue damage. Recent results suggest that carbonyl-sequestering drugs can reduce the formation of carbonylated proteins and GSH– α,β -unsaturated aldehyde derivatives and might potentially prevent or restrain carbonyl stress-associated diseases, including some of the smoking-induced gingival/periodontal tissue damage [25,68–71]. However, the potential benefits of using carbonyl scavengers in particular human diseases are still currently accompanied by a number of pitfalls and challenges confronting this therapeutic strategy [71].

Acknowledgment

This research was supported by funds provided by PUR 2009 (Programma dell'Università per la Ricerca), Università degli Studi di Milano.

Appendix A. Supplementary data

Supplementary data to this article can be found online at doi:10.1016/j.freeradbiomed.2012.02.030.

References

- [1] Pauwels, R.; Rabe, K. Burden and clinical features of chronic obstructive pulmonary disease (COPD). *Lancet* **364**:613–620; 2004.
- [2] Erhardt, L. Cigarette smoking: an undertreated risk factor for cardiovascular disease. *Atherosclerosis* **205**:23–32; 2009.
- [3] Hecht, S. S. Progress and challenges in selected areas of tobacco carcinogenesis. *Chem. Res. Toxicol.* **21**:160–171; 2008.
- [4] Bergström, J.; Bostrom, L. Tobacco smoking and periodontal hemorrhagic responsiveness. *J. Clin. Periodontol.* **28**:680–685; 2001.
- [5] Dietrich, T.; Bernimoulin, J. P.; Glynn, R. The effect of cigarette smoking on gingival bleeding. *J. Periodontol.* **75**:16–22; 2004.
- [6] Rodgman, A., Perfetti, T.A. (Eds.), 2008]. *The Chemical Components of Tobacco and Tobacco Smoke*. CRC Press, Boca Raton, FL, p. 1840; 2008.

- [7] Lu, X.; Cai, J.; Kong, H.; Wu, M.; Hua, R.; Zhao, M.; Liu, J.; Xu, G. Analysis of cigarette smoke condensates by comprehensive two-dimensional gas chromatography/time-of-flight mass spectrometry I acidic fraction. *Anal. Chem.* **75**: 4441–4451; 2003.
- [8] Pryor, W. A.; Stone, K. Oxidants in cigarette smoke: radicals, hydrogen peroxide, peroxyxynitrite and peroxyxynitrate. *Ann. N. Y. Acad. Sci.* **686**:12–27; 1993.
- [9] Pryor, W. A.; Hale, B. J.; Premovic, P. I.; Church, D. F. The radicals in cigarette tar: their nature and suggested physiological implications. *Science* **220**:425–427; 1983.
- [10] Sies, H.; Jones, D. Oxidative stress. In: Fink, G. (Ed.), 2nd ed. *Encyclopedia of Stress*, Vol. 3. Academic Press, San Diego, pp. 45–48; 2007.
- [11] Burke, A.; Fitzgerald, G. A. Oxidative stress and smoking-induced vascular injury. *Prog. Cardiovasc. Dis.* **46**:79–90; 2003.
- [12] Yamaguchi, Y.; Haginaka, J.; Morimoto, S.; Fujioka, Y.; Kunitomo, M. Facilitated nitration and oxidation of LDL in cigarette smokers. *Eur. J. Clin. Invest.* **35**:186–193; 2005.
- [13] Anderson, R. Antioxidant nutrients and prevention of oxidant-mediated, smoking-related diseases. In: Bendich, A., Deckerbaum, R.J. (Eds.), *Preventive Nutrition*, 2nd ed. Humana Press, Totowa, NJ, pp. 293–306; 2001.
- [14] Dong, J. Z.; Moldoveanu, S. C. Gas chromatography–mass spectrometry of carbonyl compounds in cigarette mainstream smoke after derivatization with 2,4-dinitrophenylhydrazine. *J. Chromatogr. A* **1027**:25–35; 2004.
- [15] Lambert, C.; McCue, J.; Portas, M.; Ouyang, Y.; Li, J.; Rosano, T. G.; Lazis, A.; Freed, B. M. Acrolein in cigarette smoke inhibits T-cell responses. *J. Allergy Clin. Immunol.* **116**:916–922; 2005.
- [16] Li, L.; Holian, A. Acrolein: a respiratory toxin that suppresses pulmonary host defense. *Rev. Environ. Health* **13**:99–108; 1998.
- [17] Eiserich, J. P.; van der Vliet, A.; Handelman, G. J.; Halliwell, B.; Cross, C. E. Dietary antioxidants and cigarette smoke-induced biomolecular damage: a complex interaction. *Am. J. Clin. Nutr.* **62**:1490S–1500S; 1995.
- [18] Andreoli, R.; Manini, P.; Corradi, M.; Mutti, A.; Niessen, W. M. Determination of patterns of biologically relevant aldehydes in exhaled breath condensate of healthy subjects by liquid chromatography/atmospheric chemical ionization tandem mass spectrometry. *Rapid Commun. Mass Spectrom.* **17**:637–645; 2003.
- [19] Annovazzi, L.; Cattaneo, V.; Viglio, S.; Perani, E.; Zanone, C.; Rota, C.; Pecora, F.; Cetta, G.; Silvestri, M.; Iadarola, P. High-performance liquid chromatography and capillary electrophoresis: methodological challenges for the determination of biologically relevant low-aliphatic aldehydes in human saliva. *Electrophoresis* **25**:1255–1263; 2004.
- [20] Aldini, G.; Dalle-Donne, I.; Vistoli, G.; Maffei Facino, R.; Carini, M. Covalent modification of actin by 4-hydroxy-trans-2-nonenal (HNE): LC-ESI-MS/MS evidence for Cys374 Michael adduction. *J. Mass Spectrom.* **40**:946–954; 2005.
- [21] Aldini, G.; Gamberoni, L.; Orioli, M.; Beretta, G.; Regazzoni, L.; Maffei Facino, R.; Carini, M. Mass spectrometric characterization of covalent modification of human serum albumin by 4-hydroxy-trans-2-nonenal. *J. Mass Spectrom.* **41**: 1149–1161; 2006.
- [22] Carbone, D. L.; Doorn, J. A.; Kiebler, Z.; Petersen, D. R. Cysteine modification by lipid peroxidation products inhibits protein disulfide isomerase. *Chem. Res. Toxicol.* **18**:1324–1331; 2005.
- [23] Dalle-Donne, I.; Carini, M.; Vistoli, G.; Gamberoni, L.; Giustarini, D.; Colombo, R.; Maffei Facino, R.; Rossi, R.; Milzani, A.; Aldini, G. Actin Cys374 as a nucleophilic target of α , β -unsaturated aldehydes. *Free Radic. Biol. Med.* **42**:583–598; 2007.
- [24] Liu, C.; Hu, J.; McAdam, K. G. A feasibility study on oxidation state of arsenic in cut tobacco, mainstream cigarette smoke and cigarette ash by X-ray absorption spectroscopy. *Spectrochim. Acta B* **64**:1294–1301; 2009.
- [25] Colombo, G.; Aldini, G.; Orioli, M.; Giustarini, D.; Gornati, R.; Rossi, R.; Colombo, R.; Carini, M.; Milzani, A.; Dalle-Donne, I. Water-soluble α , β -unsaturated aldehydes of cigarette smoke induce carbonylation of human serum albumin. *Antioxid. Redox Signal.* **12**:349–364; 2010.
- [26] Dalle-Donne, I.; Giustarini, D.; Colombo, R.; Milzani, A.; Rossi, R. S-glutathionylation in human platelets by a thiol–disulfide exchange-independent mechanism. *Free Radic. Biol. Med.* **38**:1501–1510; 2005.
- [27] Rossi, R.; Giustarini, D.; Milzani, A.; Dalle-Donne, I. Membrane skeletal protein S-glutathionylation and hemolysis in human red blood cells. *Blood Cells Mol. Dis.* **37**: 180–187; 2006.
- [28] Baty, J. W.; Hampton, M. B.; Winterbourn, C. C. Detection of oxidant sensitive thiol proteins by fluorescence labeling and two-dimensional electrophoresis. *Proteomics* **2**:1261–1266; 2002.
- [29] Giustarini, D.; Dalle-Donne, I.; Milzani, A.; Rossi, R. Low molecular mass thiols, disulfides and protein mixed disulfides in rat tissues: influence of sample manipulation, oxidative stress and ageing. *Mech. Ageing Dev.* **132**:141–148; 2011.
- [30] Aldini, G.; Granata, P.; Carini, M. Detoxification of cytotoxic α , β -unsaturated aldehydes by carnosine: characterization of conjugated adducts by electrospray ionization tandem mass spectrometry and detection by liquid chromatography/mass spectrometry in rat skeletal muscle. *J. Mass Spectrom.* **37**:1219–1228; 2002.
- [31] Griffith, O. W. Biologic and pharmacologic regulation of mammalian glutathione synthesis. *Free Radic. Biol. Med.* **27**:922–935; 1999.
- [32] Dalle-Donne, I.; Scaloni, A.; Butterfield, D.A. (Eds.), 2006. *Redox Proteomics: from Protein Modifications to Cellular Dysfunction and Disease*. Wiley, Hoboken, p. 944; 2006.
- [33] Nguyen, H.; Finkelstein, E.; Reznick, A.; Cross, C.; van der Vliet, A. Cigarette smoke impairs neutrophil respiratory burst activation by aldehyde-induced thiol modifications. *Toxicology* **160**:207–217; 2001.
- [34] Rossi, R.; Dalle-Donne, I.; Milzani, A.; Giustarini, D. Oxidized forms of glutathione in peripheral blood as biomarkers of oxidative stress. *Clin. Chem.* **52**:1406–1414; 2006.
- [35] Poggi, P.; Rota, P. R.; Boratto, R. The volatile fraction of cigarette smoke induces alterations in the human gingival fibroblast cytoskeleton. *J. Periodontol. Res.* **37**: 230–235; 2002.
- [36] Oyarzún, A.; Arancibia, R.; Hidalgo, R.; Peñafiel, C.; Cáceres, M.; González, M. J.; Martínez, J.; Smith, P. C. Involvement of MT1-MMP and TIMP-2 in human periodontal disease. *Oral Dis.* **16**:388–395; 2010.
- [37] van Beurden, H. E.; Von den Hoff, J. W.; Torensma, R.; Maltha, J. C.; Kuijpers-Jagtman, A. M. Myofibroblasts in palatal wound healing: prospects for the reduction of wound contraction after cleft palate repair. *J. Dent. Res.* **84**:871–880; 2005.
- [38] Pihlstrom, B. L.; Michalowicz, B. S.; Johnson, N. W. Periodontal diseases. *Lancet* **366**:1809–1820; 2005.
- [39] Rivera-Hidalgo, F. Smoking and periodontal disease. *Periodontol.* **2000** **2000** (32): 50–58; 2003.
- [40] Hotulainen, P.; Paunola, E.; Vartiainen, M. K.; Lappalainen, P. Actin-depolymerizing factor and cofilin-1 play overlapping roles in promoting rapid F-actin depolymerization in mammalian nonmuscle cells. *Mol. Biol. Cell* **16**:649–664; 2005.
- [41] Gross, S. R.; Kinzy, T. G. Translation elongation factor 1A is essential for regulation of the actin cytoskeleton and cell morphology. *Nat. Struct. Mol. Biol.* **12**:772–778; 2005.
- [42] Hayes, M. J.; Shao, D. M.; Grieve, A.; Levine, T.; Bailly, M.; Moss, S. E. Annexin A2 at the interface between F-actin and membranes enriched in phosphatidylinositol 4,5-bisphosphate. *Biochim. Biophys. Acta* **1793**:1086–1095; 2009.
- [43] Rescher, U.; Ludwig, C.; Konietzko, V.; Kharitononov, A.; Gerke, V. Tyrosine phosphorylation of annexin A2 regulates Rho-mediated actin rearrangement and cell adhesion. *J. Cell Sci.* **121**:2177–2185; 2008.
- [44] Dalle-Donne, I.; Rossi, R.; Giustarini, D.; Gagliano, N.; Lusini, L.; Milzani, A.; Di Simplicio, P.; Colombo, R. Actin carbonylation: from a simple marker of protein oxidation to relevant signs of severe functional impairment. *Free Radic. Biol. Med.* **31**:1075–1083; 2001.
- [45] Fedorova, M.; Kuleva, N.; Hoffmann, R. Identification of cysteine, methionine and tryptophan residues of actin oxidized in vivo during oxidative stress. *J. Proteome Res.* **9**:1598–1609; 2010.
- [46] Banan, A.; Zhang, Y.; Losurdo, J.; Keshavarzian, A. Carbonylation and disassembly of the F-actin cytoskeleton in oxidant induced barrier dysfunction and its prevention by epidermal growth factor and transforming growth factor α in a human colonic cell line. *Gut* **46**:830–837; 2000.
- [47] Banan, A.; Fitzpatrick, L.; Zhang, Y.; Keshavarzian, A. OPC-compounds prevent oxidant-induced carbonylation and depolymerization of the F-actin cytoskeleton and intestinal barrier hyperpermeability. *Free Radic. Biol. Med.* **30**:287–298; 2001.
- [48] Keshavarzian, A.; Banan, A.; Farhadi, A.; Komanduri, S.; Mutlu, E.; Zhang, Y.; Fields, J. Z. Increases in free radicals and cytoskeletal protein oxidation and nitration in the colon of patients with inflammatory bowel disease. *Gut* **52**:720–728; 2003.
- [49] Chung, W. G.; Miranda, C. L.; Stevens, J. F.; Maier, C. S. Hop proanthocyanidins induce apoptosis, protein carbonylation, and cytoskeleton disorganization in human colorectal adenocarcinoma cells via reactive oxygen species. *Food Chem. Toxicol.* **47**:827–836; 2009.
- [50] Canton, M.; Menazza, S.; Sheeran, F. L.; Polverino de Laureto, P.; Di Lisa, F.; Pepe, S. Oxidation of myofibrillar proteins in human heart failure. *J. Am. Coll. Cardiol.* **57**: 300–309; 2011.
- [51] Das, A.; Bhattacharya, A.; Chakrabarti, G. Cigarette smoke extract induces disruption of structure and function of tubulin–microtubule in lung epithelium cells and in vitro. *Chem. Res. Toxicol.* **22**:446–459; 2009.
- [52] Dalle-Donne, I.; Milzani, A.; Gagliano, N.; Colombo, R.; Giustarini, D.; Rossi, R. Molecular mechanisms and potential clinical significance of S-glutathionylation. *Antioxid. Redox Signal.* **10**:445–473; 2008.
- [53] Dalle-Donne, I.; Rossi, R.; Colombo, G.; Giustarini, D.; Milzani, A. Protein S-glutathionylation: a regulatory device from bacteria to humans. *Trends Biochem. Sci.* **34**:85–96; 2009.
- [54] Cattaneo, V.; Getta, G.; Rota, C.; Vezzoni, F.; Rota, M.; Gallanti, A.; Boratto, R.; Poggi, P. Volatile components of cigarette smoke: effect of acrolein and acetaldehyde on human gingival fibroblasts in vitro. *J. Periodontol.* **71**:425–432; 2000.
- [55] Ramu, K.; Perry, C. S.; Ahmed, T.; Pakenham, G.; Kehrler, J. P. Studies on the basis for the toxicity of acrolein mercapturates. *Toxicol. Appl. Pharmacol.* **140**:487–498; 1996.
- [56] Conklin, D. J.; Haberzettl, P.; Prough, R. A.; Bhatnagar, A. Glutathione-S-transferase P protects against endothelial dysfunction induced by exposure to tobacco smoke. *Am. J. Physiol. Heart Circ. Physiol.* **296**:H1586–H1597; 2009.
- [57] Barreiro, E.; Peinado, V. I.; Galdiz, J. B.; Ferrer, E.; Marin-Corral, J.; Sanchez, F.; Gea, J.; Barberà, J. A. ENIGMA In COPD Project. Cigarette smoke-induced oxidative stress: a role in COPD skeletal muscle dysfunction. *Am. J. Respir. Crit. Care Med.* **182**:477–488; 2010.
- [58] Morrow, J. D.; Frei, B.; Longmire, A. W.; Gaziano, J. M.; Lynch, S. M.; Shyr, Y.; Strauss, W. E.; Oates, J. A.; Roberts II, L. J. Increase in circulating products of lipid peroxidation (F2-isoprostanes) in smokers: smoking as a cause of oxidative damage. *N. Engl. J. Med.* **332**:1198–1203; 1995.
- [59] Colombo, G.; Rossi, R.; Gagliano, N.; Portinaro, N.; Clerici, M.; Annibal, A.; Giustarini, D.; Colombo, R.; Milzani, A.; Dalle-Donne, I. Red blood cells protect albumin from cigarette smoke-induced oxidation. *PLoS One* **7**:e29930; 2012.
- [60] Kelly, G. S. The interaction of cigarette smoking and antioxidants. Part I. Diet and carotenoids. *Altern. Med. Rev.* **7**:370–388; 2002.
- [61] Kelly, G. S. The interaction of cigarette smoking and antioxidants. Part 2. α -Tocopherol. *Altern. Med. Rev.* **7**:500–511; 2002.
- [62] Kelly, G. S. The interaction of cigarette smoking and antioxidants. Part III. Ascorbic acid. *Altern. Med. Rev.* **8**:43–54; 2003.

- [63] Kinnula, V. L. Focus on antioxidant enzymes and antioxidant strategies in smoking related airway diseases. *Thorax* **60**:693–700; 2005.
- [64] Stadler, N.; Eggermann, J.; Vöö, S.; Kranz, A.; Waltenberger, J. Smoking-induced monocyte dysfunction is reversed by vitamin C supplementation in vivo. *Arterioscler. Thromb. Vasc. Biol.* **27**:120–126; 2007.
- [65] Giustarini, D.; Dalle-Donne, I.; Tsikas, D.; Rossi, R. Oxidative stress and human diseases: origin, link, measurement, mechanisms, and biomarkers. *Crit. Rev. Clin. Lab. Sci.* **46**:241–281; 2009.
- [66] Goralczyk, R. β -Carotene and lung cancer in smokers: review of hypotheses and status of research. *Nutr. Cancer* **61**:767–774; 2009.
- [67] Karlsen, A.; Svendsen, M.; Seljeflot, I.; Sommernes, M. A.; Sexton, J.; Brevik, A.; Erlund, I.; Serafini, M.; Bastani, N.; Remberg, S. F.; Borge, G. I.; Carlsen, M. H.; Bøhn, S. K.; Myhrstad, M. C.; Dragsted, L. O.; Duttaroy, A. K.; Haffner, K.; Laake, P.; Drevon, C. A.; Arnesen, H.; Collins, A.; Tonstad, S.; Blomhoff, R. Compliance, tolerability and safety of two antioxidant-rich diets: a randomised controlled trial in male smokers. *Br. J. Nutr.* **106**:557–571; 2011.
- [68] Aldini, G.; Dalle-Donne, I.; Facino, R. M.; Milzani, A.; Carini, M. Intervention strategies to inhibit protein carbonylation by lipoxidation-derived reactive carbonyls. *Med. Res. Rev.* **27**:817–868; 2007.
- [69] Aldini, G.; Vistoli, G.; Regazzoni, L.; Benfatto, M. C.; Bettinelli, I.; Carini, M. Edaravone inhibits protein carbonylation by a direct carbonyl scavenging mechanism: focus on reactivity, selectivity and reaction mechanisms. *Antioxid. Redox Signal.* **12**:381–392; 2010.
- [70] Burcham, P. C.; Kaminskas, L. M.; Tan, D.; Pyke, S. M. Carbonyl-scavenging drugs and protection against carbonyl stress-associated cell injury. *Mini Rev. Med. Chem.* **8**:319–330; 2008.
- [71] Burcham, P. C. Potentialities and pitfalls accompanying chemico-pharmacological strategies against endogenous electrophiles and carbonyl stress. *Chem. Res. Toxicol.* **21**:779–786; 2008.